Key Engineering Materials
ISSN: 1662-9795, Vol. 926, pp 250-267
doi:10.4028/p-h0iapl

Submitted: 2021-11-26
Revised: 2022-03-07
Accepted: 2022-03-07
Online: 2022-07-22

The Analysis of Small-Scale Notches on the Fatigue Performance of SLM Ti-6Al-4V; A Theory of Critical Distances Approach

Bobby Gillham[1,4,a,*], Andrei Yankin[1,b], Harry Shipley[1,4,c], Fionnan McNamara[2,d], Charles Tomonto[3,e], Garret O'Donnell[1,4,f], Daniel Trimble[1,4,g], Shuo Yin[1,4,h], David Taylor[1,4,i], Rocco Lupoi[1,4,j]

[1]Trinity College Dublin, The University of Dublin, Department of Mechanical, Manufacturing and Biomedical Engineering, Parsons Building, Dublin 2, Ireland

[2]3D Printing Innovation & Customer Solutions, Johnson & Johnson Services Inc., Loughbeg, Ringaskiddy, Co. Cork, Ireland P43 ED82

[3]3D Printing Innovation & Customer Solutions, Johnson & Johnson Services Inc., Miami, Florida, USA 33126

[4]AMBER, the SFI Research Centre for Advanced Materials and BioEngineering Research, Ireland

[a]gillhamb@tcd.ie, [b]yas.cem@yandex.ru, [c]shipleyh@tcd.ie, [d]fmcnamar@its.jnj.com, [e]CTomont1@its.jnj.com, [f]ODONNEGE@tcd.ie, [g]DTRIMBLE@tcd.ie, [h]yins@tcd.ie, [i]DTAYLOR@tcd.ie, [j]lupoir@tcd.ie

Keywords: Fatigue modelling, LEFM, Notches, Surface effects, Critical distance

Abstract. Selective Laser Melting is an additive manufacturing practice that permits the production of metal alloy-based parts. While facilitating the design of complex geometry, SLM leads to the fabrication of a unique material structure that showcases distinct behavioural characteristics relative to their traditional methods of material manufacture. Defects that are innate to SLM inspire the presence of a compositional outlook that is inhomogeneous in nature and only serves to hinder part efficiency. Thus, the Theory of Critical Distances offers a refreshed proposal to evaluating notched Ti-6Al-4V material produced by additive manufacturing processes. Key principles of the theory's working mechanisms are outlined. Subsequently, symmetrical notches of contrasting size are assessed. Findings reveal that the Theory of Critical Distances is adequately compatible with accurate fatigue prediction of SLM Ti-6Al-4V in its as-built state. Additionally, fracture surface analysis reveals that crack initiation is predominantly a surface-based phenomenon. Hereby, increased focus must be given to the quality of processed material that is located at the externalities of additively manufactured components, in order to enhance their service life capabilities. This will induce an increasingly uniform material structure that will allow for more predictable behavioural characteristics.

Introduction

Selective Laser Melting (SLM) is a method of additive manufacturing (AM) that is classified under the realm of being a laser-based powder bed fusion process [1]. The prominence of metal AM methods has more recently become a mainstay feature of niche manufacturing techniques. Primarily dedicated to the escalation of technology in key departments, the provision for enhanced recognition and finer control of the process as a whole has been enabled. Such growth has catered for the process' capability to engineer components with complex shapes. Moreover, a short design-to-manufacture cycle time and the ability to produce customized components from a wide range of materials can be availed of. Herein, metal alloys such as Ti-6Al-4Vthat possess high strength-to-weight ratios along with other exceptional material properties, are employed [1].

Notwithstanding its continuing emergence, the SLM technique fails to subdue the numerous sources of material defects that are so often attributed to the field of AM. More specifically, an α' martensitic microstructure, residual stresses, surface roughness and process inherent porosity are all indicative of AM Ti-6Al-4V in the as-built format [2]. The spontaneous locality of material inherent weaknesses can promote the degradation of mechanical properties. These frailties undermine

resulting material characteristics in comparison to those of their conventionally manufactured counterparts, as highlighted by [3].

Sighting the endorsement of AM Ti-6Al-4V material within environments through which an elongated and trustworthy service lifetime is indispensable, a strong knowledge of fatigue behaviour is essential. Within existing literature, multiple studies have taken an experimentally-heavy based approach to identifying the potential of AM Ti-6Al-4V in this regard. The potential influence of porosity [4–6], surface roughness [7–9], microstructure [10,11] and residual stresses [12,13] on the reduction of fatigue performance have all been critiqued. Granted however, the nature of regulated fatigue investigations can inevitably become time-consuming and exhausting. It is for this reason that such engagements often prove to be impractical.

Accounting for this, the ideation of assessing a material's performance through an alternative medium of theoretical prediction is one that continues to gain significant traction. Ti-6Al-4V in the field of AM is predominantly characterised by its high strength and low ductility. Hence, the dynamic performance can be well portrayed via the sole consideration of elastic material behaviour [14]. Moreover, the application of stress concentrations that have been inferred through design are necessary to comprehend in respect to the response of subsequent material mannerisms. Within the scope of AM, the reason for this is twofold. Hereby, the ability to assess a material's performance under stress concentrations that have been induced by complex shapes remains essential. Additionally however, the presence of process-inherent material defects that are typically associated with SLM materials also have the potential to give rise to such stress raising locations within part composition. Consequently, it is of critical value to have an in-depth understanding of exactly how such geometrical and process-inherent material anomalies may have a combined impact upon component service life.

One potential approach upon which forecasting the fatigue resistance of AM metal alloys can be made is through the utilisation of a simple 'hot spot' method (Fig. 6(a)). Herein, the maximum stress experienced at the tip of a notch is surveyed. Yet, fundamental applications of such a strategy reveal that somewhat conservative evaluations are too often made. Subsequently, adaptations to the 'hot spot' hypothesis have been generated. Neuber[15] and Peterson [16] proposed Line (LM) and Point (PM) methods respectively, with the conception that a critical volume of material must be exposed to a critical stress as a prerequisite for fatigue to transpire. Parallel works in this domain led to the establishment of definitively linking such methods to Linear Elastic Fracture Mechanics (LEFM) principles [17]. Further developments by multiple authors [18,19], that were also related to independent research by Tanaka et al. [20], resulted in a concrete definition of the Theory of Critical Distances [21].

Within the realm of developing theories to make predictions on the phenomena of brittle fracture and fatigue, such approaches can be broadly divided in to two categories; mechanistic models and continuum mechanics models [21]. The TCD concept incorporates elements from both of the aforementioned model types. It is referred to as a modification of LEFM whereby the existence of mechanisms at the microstructural level is represented by the introduction of a single length scale parameter, L. Primary motivation behind the development of a modified LEFM was to overcome the difficulty in quantifying short crack behaviour. This followed the discovery of the tendency for short cracks to deviate from the standard expectations of materials conforming to LEFM. This is due to such small cracks being open to behavioural influences from local microstructure.

It should be realised that the TCD is not the only fatigue prediction theory known to exist within the domain of modified fracture mechanics. Notably, El Haddad et al. [22] modified the LEFM equation to include an additional constant, a_0. In doing so, their approach essentially assumed crack behaviour to play out as if the crack in question was longer by a length equal to a_0. Hereby, the laws of LEFM remained applicable. Distinct similarities can be made here between the value of $a_0$and that of 'L' which is used in TCD methods.

Elsewhere, Murakami composed a technique to analyse the impact of small defects within metals [23]. It relies on modelling the effective size of a defect as the square root of the area to which it projects on to a plane that is normal to the axis of applied stress. Given its perceived suitability to

model the presence of porosity within AM metallic materials, its application to-date can be seen as significant with respect to predicting fatigue capabilities of such inherently porous materials. As a case in point, Zhang et al. exercised its use to predict the fatigue strength of AM Ti-6Al-4V based on quantifying the stress intensity factor of crack initiating defects [24]. Hu et al. employed the combined use of the Murakami model and statistics of extremes to evaluate the fatigue performance of SLM Ti-6Al-4V in terms of defect population [25]. Nevertheless, Murakami's method lacks in the ability to assess extreme values. For large defects that behave like a macroscopic notch or crack, the $\sqrt{area}$ parameter falls short in its analysis potential. Likewise, the same can be said for infinitely small defects that are not responsible for the onset of fatigue failure. In comparison, TCD methods hold true under the consideration of any defect size.

The topic of fatigue in AM of Ti-6Al-4V material is well addressed in the current state-of-the-art literature. Amongst the numerous sub-divisions of this field, the anatomy of notched specimens remains bare. However, intensifying the focus around notched phenomena offers a promising path towards unveiling the precise impact that AM material defects, particularly in the form of porosity and surface roughness, can impose on dynamic mechanical part performance. In view of this, Ravazi et al. quantified the response of both smooth circular and V-notched geometries to cyclic loading sequences [26,27]. A distinct priority was made towards identifying crack initiation and failure mechanisms of these parts. Ravazi also employed the use of notched specimens in another separate review [28]. Herein, an evaluation surrounding the effect of AM part thickness in tandem with its geometry was conducted. Nicoletto et al. questioned the impact of build direction on the fatigue of notched Ti-6Al-4V samples, whereby a link was established between it and resulting fatigue notch sensitivity [29]. Elsewhere, Kahlin et al. observed fatigue properties for both laser sintered and EBM Ti-6Al-4V, whereupon the effects for a combined rough as-built surface and a geometrical notch were established [30]. Witkin et al. also explored the potential for considering a rough as-built surface as a notch [31]. Finally, Benedetti [32], Van Hooreweder [33] and Zamzami [34] currently represent the only other authors of note to involve the use of critical distance theory in investigations of notched SLM Ti-6Al-4V material. The prevailing message within each of their works reported upon the satisfactory accuracy levels of TCD results. However, the extent of notch geometries scrutinised was somewhat restricted, especially with regards to the range of notch root radii considered.

TCD methodologies have been experimented with on a range of materials and failure modes since their enouncement. A select few studies have centred upon the topic of brittle fracture via fatigue of traditionally manufactured Ti-6Al-4V. Herein, the application of TCD towards conventionally produced titanium alloy was exercised [35–37]. All publications deliberate the possibility for a critical distance size effect to persist. It is suggested that such a phenomenon may exist, whereby reducing the radius of the notch root subsequently leads to a smaller critical distance value (L) being obtained. Herein, in this particular case, they argue that the TCD may not be accurately applicable. Therefore, this poses the question as to whether the same effect may also be experienced through the application of TCD methods to AM Ti-6Al-4V material.

This study aims to expand on initial findings that were made in [38], in an attempt to further explain, quantify and engage with the suitability of TCD principles in the High Cycle Fatigue (HCF) regime for both geometrically-induced notches and process-inherent defects. Determination of two key material constants that are necessary for the TCD approach are revealed. Formulation of TCD predictions are compared alongside experimental S-N data for both plain and notched flat fatigue specimens. Via collating the predictability of performance for both macro and micro scale notched specimens alongside each other, an assessment is made on whether the TCD is appropriately applicable to those components with a characteristically irregular SLM surface topology being modelled as a micro-notch. An expanded study of results then succeeds. This includes the analysis of variation in critical distance parameter, L, with fatigue life and notch geometry. The perceived accuracy of TCD predictions are discussed in more detail. Finally, preliminary fracture surface revelations are built upon to better understand the onset of fatigue in both plain and notched AM Ti-6Al-4V material.

Materials and Methods

Sample production by SLM. The production of fatigue samples was conducted via the SLM process on a Realizer SLM 50. Titanium alloy Ti-6Al-4V ELI (Grade 23) powder was selected as the material of choice. Metal powder particles were formulated by plasma atomisation and acquired geometry of a spherical nature (Fig. 1(b)). Fig. 1(a) illustrates the particle size distribution, as measured using the laser diffraction technique via a Malvern Mastersizer 3000. A D90 ≤ 47.2 µm was recorded. All components underwent processing of their bulk material through a constant allocation of process parameters; P=95 W, v=300 mm/s and h=80 µm. A contour scan around the peripheral layer of material differed in scan settings, with P=32 W and v=250 mm/s. Each scanned layer alternated via a 45° rotation and its thickness held a value of 25 µm. Processing occurred under an inert atmosphere of Argon gas. Purging of the build chamber transpired at a set gas flow rate of 60 L/min.

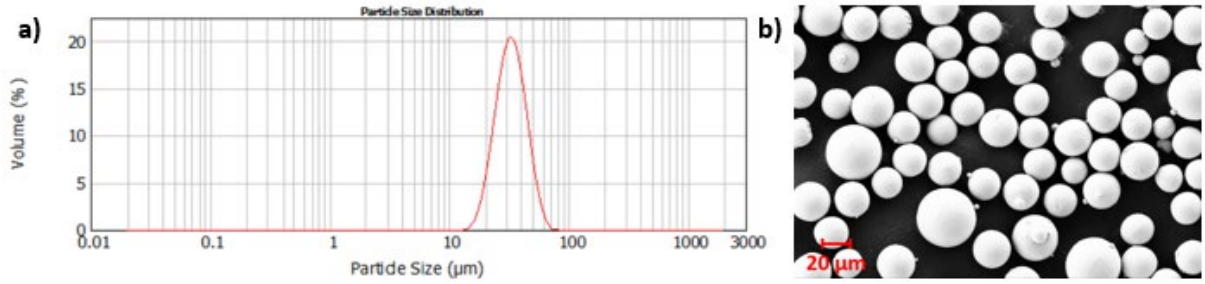

Figure 1 - a) Powder particle size distribution via laser diffraction and b) SEM image of Ti-6Al-4V powder

Regular fatigue specimens were designed with a rectangular cross-section (Fig. 2(a)). Their dimensions conformed to the geometrical standards of ASTM E466-15. With regards to their notched counterparts, a structured configuration involving notch depth (D), notch radius (ρ) and notch angle (Θ) is portrayed in Fig. 2(b). Specific trigonometry for each implemented design iteration and its subsequent stress concentration factor (Kt) is outlined in Table 1.

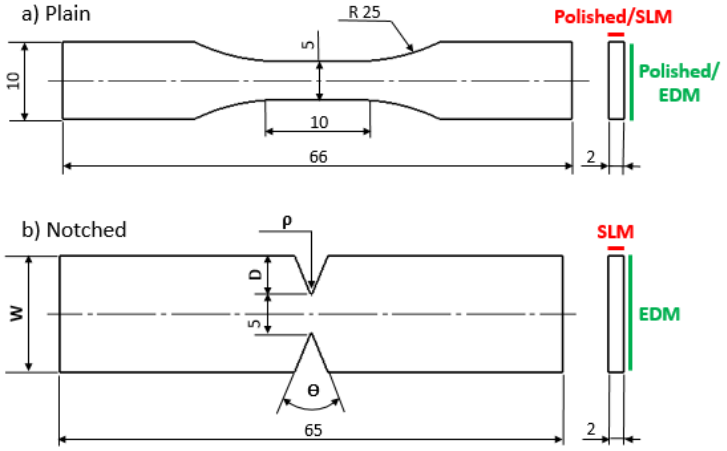

Figure 2 - Designed geometry for a) Plain fatigue specimens and b) Notched fatigue specimens

Table 1 - Overview of specimen geometry and surface condition

Specimen Type	D [mm]	ρ [mm]	W [mm]	Θ [°]	Kt	Surface Condition
Plain	N/A	N/A	10	N/A	1	Polished
Notched	5	5	15	N/A	1.31	SLM/EDM
Notched	5	1	15	45	2.3	SLM/EDM
Notched	5	0.1	15	45	6.72	SLM/EDM
Notched	0.3	0.1	5.6	45	4.21	SLM/EDM
Notched	0.1	0.1	5.2	N/A	2.93	SLM/EDM
Plain	0.06	0.005	5.12	20	5.51	SLM/EDM

At the outset, incisions with a significant depth (D=5 mm) profile were produced. Following that, a progressively decreasing notch size was imposed upon each successive design iteration. Consequently, the shallowest geometrical indentation (D=0.1 mm, ρ=0.1 mm) converged on acquiring features of a similar magnitude to those present on an inherently rough SLM surface (Fig. 3). Furthermore, plain fatigue samples containing an as-made SLM surface texture were modelled under the imposition of a micro-notch. More detail on this procedure is disclosed in 'Sample Characterization'. For each specimen type defined in Table 1, one sample of considerable thickness was manufactured in a horizontal configuration relative to the build platform. Succeeding the formation of one excessively broad sample, several parts of 2 mm thickness were segmented from the initial bulk component via wire EDM. With the exception of one plain specimen sample set, no post-process operations were executed upon the original as-made SLM surface condition. With reference to the discrepant set, a rough SLM exterior endured polishing until an Ra in the range of 1-2 µm was obtained.

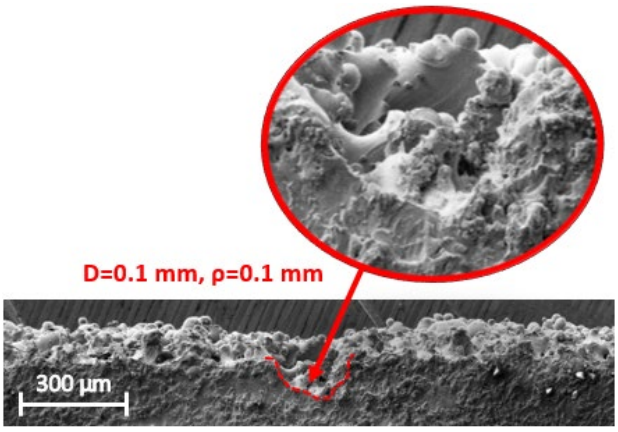

Figure 3 - Smallest notch size approaching surface topology versus a regular SLM surface

Sample Characterization. In accordance with ASTM standard B962-17, the evaluation of part density via Archimedes approach served as an indication towards the magnitude of process-inherent defects that were present throughout the bulk material. Relative density measurements returned an average value of 99.4%. As a way of verifying this result, visual analysis of one typical fatigue specimen took place using SEM examinations. 2D cross-sections of sample material exposed similar information, whereby little porosity was evidently present throughout part composition. More specifically, minute proportions of porosity were situated in the bulk material. Herein, only gas pores of an extremely small size were evident, while lack of fusion (LoF) type voids were seldomly located. Nevertheless, LoF defects did prevail with more frequency at part peripheries, often situated either at the surface level or otherwise immediately below it.

Occupying the sub-surface region, Fig. 4(a) highlights an example of the typical LoF defect style that dominates within manufactured SLM entities. An irregularly shaped pore outline is connected to the component's exterior via a crack-like criterion. Furthermore, it's random nature is complimented by a characteristically rough and irregular surface condition that remains on the part's exterior following the SLM process. Process-inherent deficiencies such as that shown in Fig. 4(a) serve as a prime exemplary as to the dominant form of material anomalies observed within test subjects.

Fig. 4(b) identifies an α' martensitic microstructure that is indicative of SLM Ti-6Al-4V substances in their as-built format. This arises as a direct consequence of the high cooling rates associated with laser-based powder bed fusion operations. Primary α grains of a needle-like appearance form at an angle of ±45° to the vertical build direction. Such an arrangement of grain positioning is resemblant of the crystallographic planes of preferential growth. Supplementary to primary α grains, secondary phase α grains promote themselves amongst the overall microstructural configuration. Stimulated by the cyclical nature of constant heating and cooling sequences throughout production, they represent grains of a comparative shape but significantly reduced in size to their

primary α counterparts. A microstructural architecture that is classified as being predominantly martensitic contributes to purveying material mannerisms whereby the mechanism of failure is fundamentally brittle in nature.

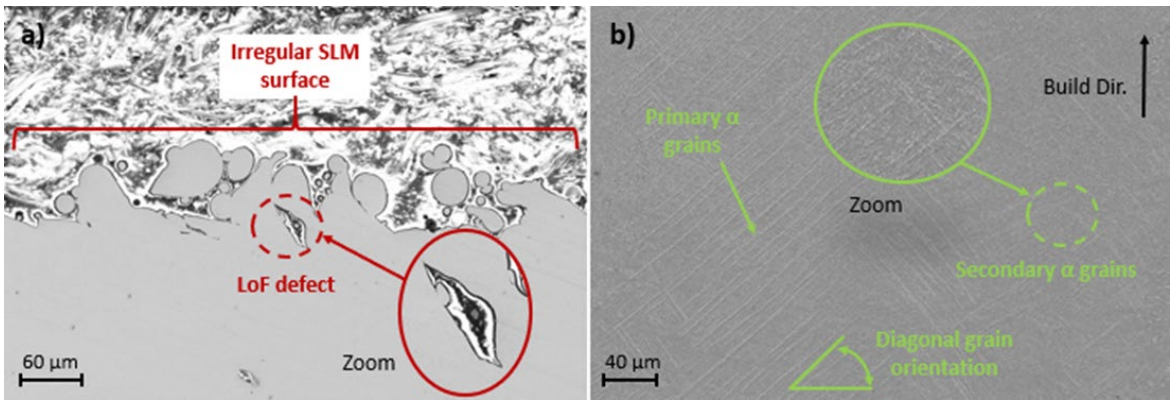

Figure 4 - (a) An illustration of porosity-inspired sub-surface defect mechanisms for SLM material in its as-built state with an irregular SLM surface condition and (b) Needle-like martensitic α-dominated microstructure associated with SLM specimens

Accounting for the necessity of modelling a characteristically coarse SLM surface as a micro-notch for TCD purposes, an accurate assessment of the exact surface texture was required. Hence, in alignment with recommendations of ISO 4287:1997, 2D profilometry quantified its precise nature via a Mitutoyo Surftest SJ-400 device (Fig. 5). Additionally, a three-dimensional graphic provided enhanced visualization of the overall as-made SLM façade. An Olympus DSX1000 digital microscope enabled an alternative non-contact appraisal of the surface condition (Fig. 5). With regards to the externalities of fatigue specimen sets whereupon a distinct SLM texture remained (ref. Fig. 2), 2D profilometry indicated an average Ra of 11.84 µm and Rz of 76.27 µm. Elongated boundary lengths (Fig. 2) ascertained refined roughness values that were influenced via a direct result of the wire EDM dissection of components from the original bulk material piece. EDM imposed a texture upon the periphery that was denoted by an Ra of 3.14 µm and Rz of 22.03 µm. For the objective of devising TCD-based simulations of an as-built SLM surface condition, the depth profile associated with such an external texture is also of key concern. This emanates from the apparent pertinence of valley depth (Rv) to be contemplated as a sharp crack [30]. Therefore, inspired by the measured 2D profile shown in Fig. 5, notch depth (D) was set as 60 µm during the process of imposing FEA on plain fatigue specimens that possessed an uneven SLM surface. Owing to revelations of a microscopic evaluation, notch radius (ρ) was assigned a value of 5 µm (Table 1).

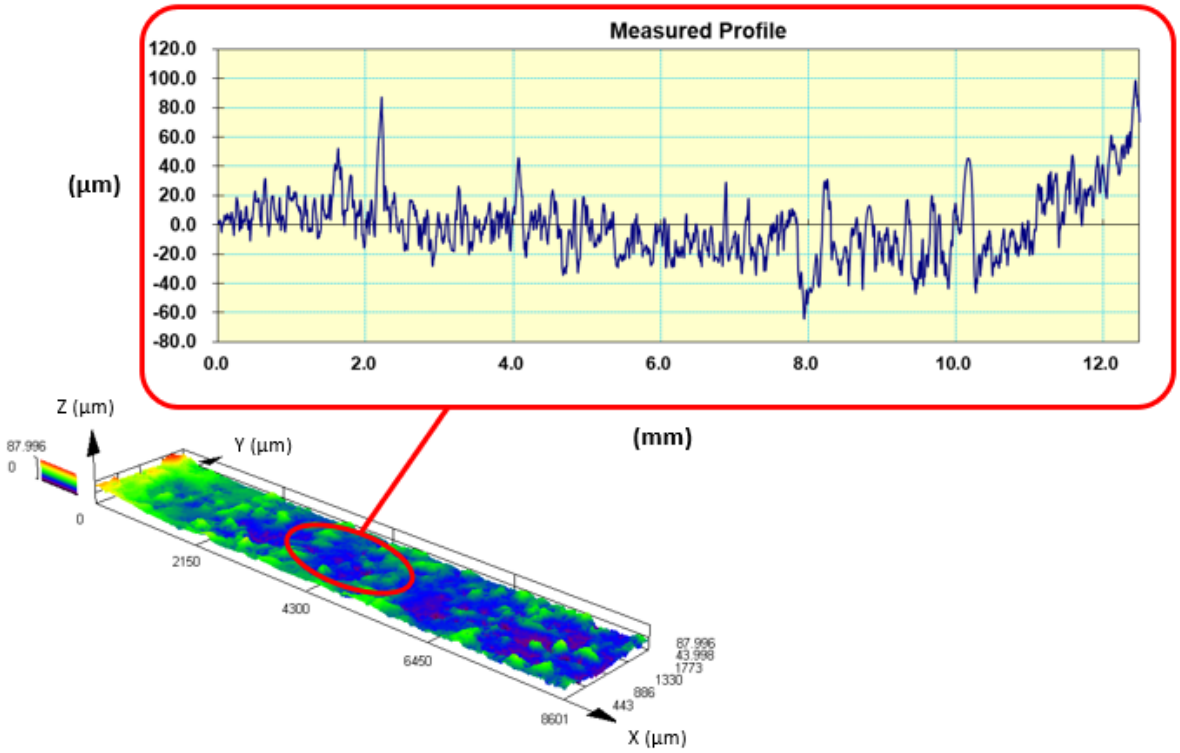

Figure 5 - A representative 3D image and 2D surface profile of a regular SLM surface associated with unpolished plain fatigue specimens

Mechanical Testing and Fatigue Data Analysis. The experimental procedure followed during fatigue loading of all test specimens is documented as follows. Herein, cyclical loading in the axial plane occurred via an INSTRON 8801. A load ratio of R=0.1 provided for tension only constant amplitude loading at a frequency of 15 Hz.

As illustrated in Fig. 8 in the form of a Wöhler curve, experimental data for each plain specimen with a polished surface condition was combined for the purpose of constructing a stress-cycle (S-N) curve. A condensed amount of trials were conceived with regards to notched designs, whereby the outcome of each cyclic loading inspection was plotted in the form of an individual data point (Fig. 8). Among each specimen design type, data was recorded over a range of $10^4 - 2 \times 10^6$ cycles. In the absence of part failure arising prior to the point of 2×10^6 cycles being reached, the test was denoted as a run-out.

The acquired experimental data was evaluated in the form of its stress-cycle relationship. Hereafter, predictive analysis on the service life of notched components was outlined via the practice of the Theory of Critical Distances (TCD).

TCD Methodology. TCD practices are built on the foundations of LEFM [21]. It is a group of methods that operates on one basic advancement; the stress of a representative point or line in the region of a notch is considered. Estimation of component failure is said to arise when the stress at a point or the average over a range of distance from the notch tip surpasses the fatigue strength of the material in question. TCD-based investigations in this study focus on those of the Point (PM) and Line (LM) method techniques, as shown in Fig. 6 (c) & (d).

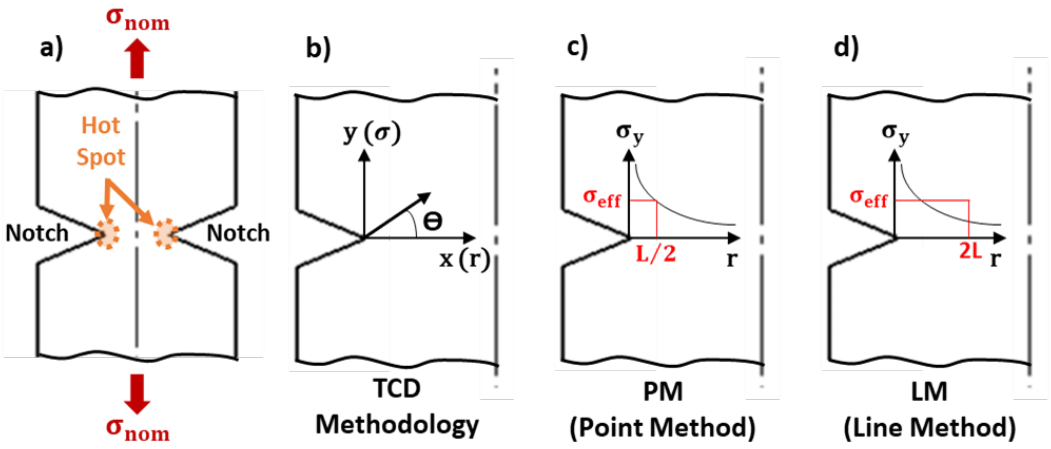

Figure 6 - a) Experimental outline with applied load direction and regions of interest – b) Principles of TCD methodology, c) Point (PM) and d) Line (LM) Methods

Each approach is defined by their respective Equations (1 & 2).

Point Method:

$$\sigma_{eff} = \sigma_0 = \sigma_y\ (\theta = 0, r = L/2) \tag{1}$$

Line Method:

$$\sigma_{eff} = \frac{1}{2L}\int_0^{2L} \sigma_y\ (\theta = 0, r)\ dr = \sigma_0\ (LM) \tag{2}$$

Where,
σ_{eff} = effective stress
$\sigma_y(r)$ = stress-distance curve for notched specimen
σ_0= fatigue strength for plain specimen
L = critical distance

The critical distance, L, is a constant that is material specific. It is also dependent upon the load ratio, R, and fatigue life, N. For a given fatigue life, it can be defined by the following equation:

$$L = \frac{1}{\pi}\left(\frac{\Delta K_{th}}{\Delta\sigma_0}\right)^2 \tag{3}$$

Where,
ΔK_{th}= threshold stress intensity range for fatigue crack growth in the material

In order to compare experimental data with TCD predictions, stress-distance curves are acquired via static FEA simulations by using ANSYS Workbench 2020 R2. Fig. 7(a) illustrates a typical example of a finite element (FE) mesh used to model SLM notched specimens. For each specimen, a main body mesh element size of 0.5 mm was used. However, a refined mesh was located around the edge of the notch to achieve a stress analysis of high precision in this location. Hereby, this region of interest was defined by an initial element size of 0.02 mm (20 µm) at the notch tip, with a subsequent growth rate of 1.05 in to the immediately surrounding bulk material (Fig. 7(a)). Utilisation of such parameters proved sufficient to give accurate stress-distance information in the critical region of interest.

Material properties (Young's Modulus and Poisson's ratio) were selected from the ANSYS library for AM Ti-6Al-4V material. One end of the specimen model was restrained via a fixed support, while a given tensile load was applied at the opposite end. The applied load was calculated as a product of the maximum stress and minimum cross-sectional area. With regards to the maximum applied stress, it corresponds to that which was associated with each individual data point in the case of both notched and unpolished flat plain specimens (Fig. 8). Alternatively, critical stress, σ_0, assimilates to the equivalent stress for the same number of cycles to failure, taken from the line of best fit to the experimental Wöhler curve. Depicted as the blue line in Fig. 8, it is formulated on the basis of experimental data obtained from plain fatigue specimens with a polished surface (Fig. 2(a)).

To allow for the implementation of TCD analysis, the linearized maximum principal stress (Fig. 7(b)) was recorded as a function of distance from the notch tip, along a horizontal line that protrudes directly inwards from the notch tip and in to the surrounding bulk material behind (Fig. 7(c)). Accounting for the fact that this line of interest is oriented perpendicular to the applied stress, it provides an overview of stress distribution within the most highly stressed region of the part. Using data from the stress-distance curve, $\sigma_y(r)$, and the appropriate plain specimen fatigue strength, σ_0, critical distance, L, could then be calculated according to both the PM and LM. Fig. 7(d) outlines the calculation of 'L' for both Point and Line methods of the TCD. In this particular case, values correspond to that of one of the most severely notched specimens (5x0.1 mm – No.2). The same procedure is followed for all test components. Computational values of 'L' (Table 2) and subsequent error margins for TCD based predictions (Table 3) are outlined in the 'Results and Discussion' section.

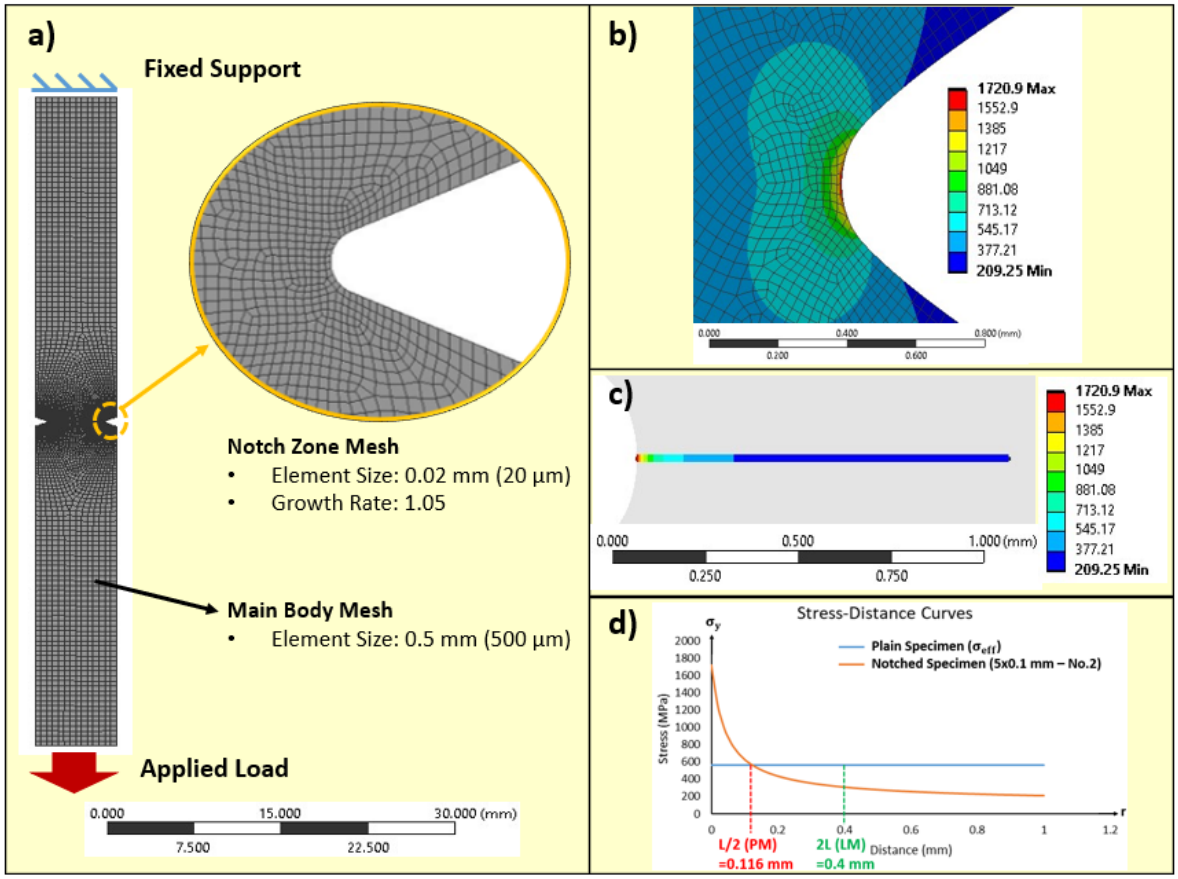

Figure 7 - a) Overview of model setup in ANSYS Mechanical, b) FEA of maximum principal stress distribution surrounding notch tip, c) Maximum principal stress distribution perpendicular to applied tensile load, along a line extending from the notch tip & d) Formulation of a stress-distance curve using stress data displayed in (c)

Results and Discussion

Experimental Fatigue Data and Determination of Critical Stress, σ0. Fig. 8 shows the data points of all experimental fatigue results in log scale format from each set of samples examined. A Wöhler curve that is constructed from the data set of polished plain fatigue specimens is presented. Wöhler curves were plotted using a power function (Eqn. 4) which is described as a line in terms of the logarithmic scale:

$$\sigma_{max}(N) = aN^b \tag{4}$$

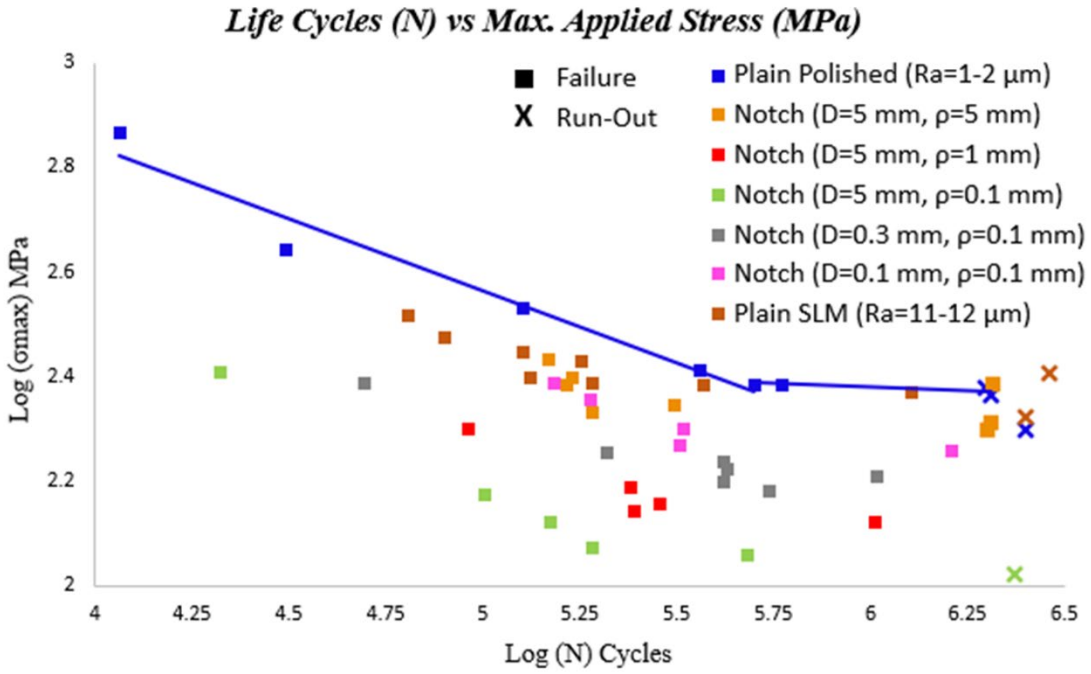

Figure 8 - Experimental fatigue data for both plain and notched specimens as outlined in Table 1

Critical stress (σ_0) is determined from the S-N curve of the plain polished specimen set at any given point (Fig. 8).

Determination of Critical Distance, L

Critical Distance vs Fatigue Life. Using both PM and LM approaches as previously defined, critical distance values were computed for all of the experimental points corresponding to notched specimens (Table 1). Table 2 summarises computed values of L for each experimental data point. With reference to two individual points that relate to the 5x5 (D=5 mm, ρ=5 mm) notched specimen type, it is noted that critical distance values are listed as being equal to 0. This scenario occurs due to the failure of an intersection point arising between the stress-distance curves of both the notched component (5x5) in question and the polished plain specimen at the associated fatigue lives. All values of L (PM & LM) are plotted against their corresponding fatigue lives on a logarithmic scale (Fig. 9(a)). A line of best-fit indicates the relationship between critical distance, L, and fatigue life for both PM and LM techniques. Visually, it depicts minimal change in L as fatigue life increases. Follow-up regression analysis in the form of a t-test confirms that, at a significance level of α=0.05, there is no statistically significant relationship present.

A similar relationship between critical distance, L and fatigue life was noted in Fig. 3 of [34]. Concerning the case of R=0.1, it is evident that variation of L with fatigue life, N, is very little. Hereby, in agreement with conclusions made in this study, the hypothesis was formed that 'critical distance could be taken as constant and equal to its value averaged over the fatigue lifetime interval of interest'. Authors recorded a uniform distribution of predictions using LM, with PM and Area Method approaches proving to give a more conservative outlook.

Table 2 - Critical Distance values according to PM and LM

Specimen	Fatigue Life (N)	Log (N)	Critical Distance, L		Avg. L (PM) [mm]	Avg. L (LM) [mm]
			L(PM) [mm]	L(LM) [mm]		
5x5 (No.3)	147367	5.1684	0.472	0.243		
5x5 (No.4)	168668	5.22703	0.196	0.102		
5x5 (No.5)	163836	5.21441	0.000	0.000	0.231	0.121
5x5 (No.6)	311561	5.49354	0.485	0.258		
5x5 (No.8)	191438	5.28203	0.000	0.000		
5x1 (No.1)	90987	4.95898	0.247	0.129		
5x1 (No.6)	238312	5.37715	0.231	0.131		
5x1 (No.2)	285757	5.456	0.222	0.119	0.217	0.121
5x1 (No.4)	243254	5.38606	0.106	0.066		
5x1 (No.3)	1020637	6.00887	0.277	0.161		
5x0.1 (No.2)	20894	4.32002	0.233	0.200		
5x0.1 (No.1)	100190	5.00082	0.193	0.158		
5x0.1 (No.4)	147800	5.16967	0.200	0.154	0.212	0.173
5x0.1 (No.6)	190222	5.27926	0.173	0.137		
5x0.1 (No.5)	480506	5.6817	0.259	0.215		
0.3x0.1 (No.6)	49528	4.69485	0.129	0.113		
0.3x0.1 (No.1)	208850	5.31983	0.182	0.143		
0.3x0.1 (No.3)	417840	5.62101	0.237	0.219		
0.3x0.1 (No.4)	418263	5.62145	0.197	0.176	0.196	0.174
0.3x0.1 (No.5)	427680	5.63112	0.209	0.204		
0.3x0.1 (No.7)	584894	5.76708	0.207	0.157		
0.3x0.1 (No.2)	1036940	6.01575	0.212	0.207		
0.1x0.1 (No.1)	151142	5.17939	0.130	0.129		
0.1x0.1 (No.2)	188073	5.27433	0.136	0.115		
0.1x0.1 (No.6)	320714	5.50612	0.113	0.096	0.141	0.123
0.1x0.1 (No.3)	328574	5.51663	0.165	0.131		
0.1x0.1 (No.5)	1602275	6.20474	0.160	0.145		

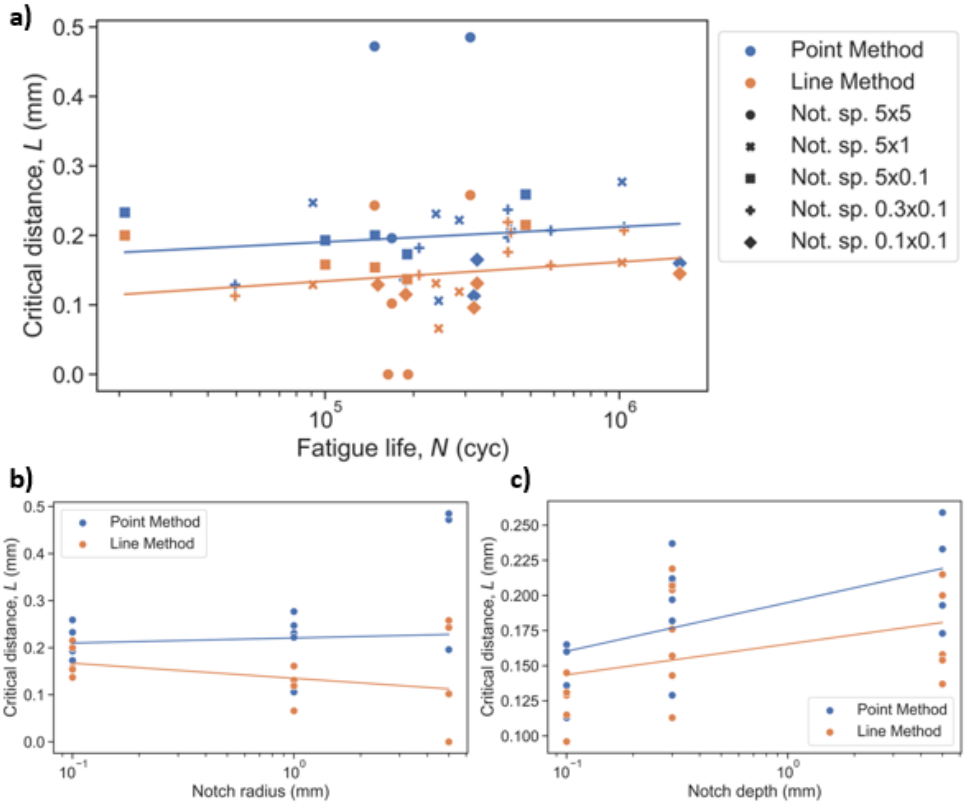

Figure 9 - Relationship between critical distance, L, and a) fatigue life, b) notch radius, c) notch depth

Critical Distance vs Notch Geometry. It has previously been mentioned in literature that critical distance, L, may be a function of notch geometry [35–37]. In an attempt to establish whether any such correlation may exist, L was plotted against both notch radius (Fig. 9(b)) and notch depth (Fig. 9(c)). Once again, regression analysis verified the potential for any statistical significance to exist.

Concerning the variation of L with notch radius, no influential level of association was found. On the other hand, a statistical t-test indicated a correlation to be present between L and notch depth, at a significance level of α=0.05. Herein, at the specified significance level, L was found to increase with notch depth. This held true in the case of the PM only.

TCD Predictions (PM and LM)

Computation of Critical Distance, L. In agreement with common practices from literature [21], TCD methods are frequently conducted in engineering design via the computation of L in a certain manner. This involves exploitation of stress-distance curve data from two contrasting specimen designs only; polished plain components and those that are most severely notched (5x0.1 mm). Via such an approach, average values of critical distance were determined to be $L_{PM} = 0.212$ mm and $L_{LM} = 0.173$ mm respectively for each of the TCD techniques considered. Subsequent TCD predictions were formulated through both PM and LM avenues, with results outlined in Table 3. Specimens denoted as 'SLM Plain' refer to those that possessed an irregular SLM surface but no additional geometrically induced notch.

As a point of note, it could be argued that the most accurate values of L may be arrived at by averaging values from all specimens, as outlined in Table 2. The adoption of this alternative returns results of $L_{PM} = 0.199$ mm and $L_{LM} = 0.145$ mm. This is contrary to the approach which was taken in this study, whereby average L values were taken from the most severely notched (5x0.1 mm) specimen set only for the purpose of making predictions. Nevertheless, it is worth noting that other options to determining an averaged L value are available. Going forward, further exploration of such modifications may be worth exploring in an effort to determine the most accurate TCD approximations.

Average Absolute Error. On account of the average absolute error (%), Table 3 illustrates a reduced error margin for larger notched components ($\mathbf{D \geq 0.3\ mm}$) for both TCD approaches. Appraisal of smaller notched specimen data ('0.1x0.1' and 'SLM Plain') indicates further transgression in the predictability of their fatigue performance however. This holds true with respect to the PM method only and is owed to values of L significantly decreasing with notch depth in this scenario (see Table 2). With reference to plain specimens containing an inherently rough SLM surface texture, it is recalled that such parts were modelled as a micro-notch (D=60 μm, ρ=5 μm) to enable the application of TCD predictions. A maximum average absolute error of 16.11 % was obtained using the PM method; maximum errors of a select few data points exceed 20% only for 0.1 x 0.1 notched and SLM Plain specimens, solely with regards to use of the PM. According to LM, maximum errors for each specimen are below 20 %; fatigue prediction errors that are < 20 % are widely accepted. Therefore, LM is more preferable than PM in this scenario.

Standard Error of the Estimate. To further assess the predictive ability of both TCD methods, the standard error of the estimate (SEE) can be considered (Eqn. 5). By performing such an analysis in terms of the logarithmic scale which was used to formulate the Wöhler curve (Fig. 8), SEE of the regression line may be regarded as the experimental error (SEE(Exp.)). Hereby, discrepancies between experimental data points for the polished plain specimen set and the subsequent Wöhler curve that was formed, are accounted for. SEE of TCD predictions for both PM and LM approaches may then be quantified as the error that is associated with the TCD models themselves. In doing so, error margins between each experimental data point and their corresponding PM and LM estimations are ascertained. SEE is calculated as follows:

$$SEE = \pm\left(10^{\sqrt{\frac{\sum_{i=1}^{n}(log(\sigma_{mod}/\sigma_{exp}))^2}{n-2}}} - 1\right) \times 100\ \% \tag{5}$$

Where,

n = No. of experimental points (data set size)

σ_{mod} = Max. stress acquired via power function (Eqn. 4) for experimental error **or** Max. stress acquired via TCD predictions (PM/LM) for model error

σ_{exp} = Max. experimental stress for each individual data point

Using data from polished plain specimens and the corresponding Wöhler curve, SEE(Exp.) is computed to be equal to 9.54%. Therefore, it is assumed that any error margin for SEE of TCD predictive models that falls within a similar range of SEE(Exp.) is indicative of a satisfactory model performance. On reflection of both SEE(PM) and SEE(LM) for each specimen set (Table 3), SEE of each technique only deviates slightly from that of SEE(Exp.), apart from one exception. TCD predictions made for smaller sized notches according to the PM only produced a greater amount of error. With regards to 0.1x0.1 mm notched specimens and the plain specimen type with an irregular SLM surface, SEE(PM) rises considerably to 19.6% and 21.5% respectively. Thus, it is proposed that the PM may not be capable of predicting the fatigue performance of smaller notched specimens that are beyond a certain size limit. Such trends are also in agreement with those of the average absolute error margins. Reasoning for reduced accuracy of the PM in this regard can be referenced back to evidently decreasing values of critical distance (L) for cases where notch depth is significantly decreased (ref. Table 2).

Table 3 - Average absolute and standard error of the estimate error margins of predicted fatigue strength values according to PM and LM for each specimen data set

Specimen Type	Data Set Size	Avg. ABS Error [%] PM	Avg. ABS Error [%] LM	SEE (PM) [%]	SEE (LM) [%]
Notch (D=5 mm, ρ= 5 mm)	5	4.05	5.77	8.7	9.83
Notch (D=5 mm, ρ= 1 mm)	5	3.53	7.26	5.76	11.08
Notch (D=5 mm, ρ= 0.1 mm)	5	6.75	7.05	10.21	10.17
Notch (D=0.3 mm, ρ= 0.1 mm)	7	6.93	6.37	10.38	9.51
Notch (D=0.1 mm, ρ= 0.1 mm)	5	14.53	8.08	19.65	11.4
Plain SLM (D= 60 µm, ρ=5 µm)	8	16.11	7.67	21.5	11.71

Fracture Surfaces. SEM analysis of fracture surfaces in the slow fracture fatigue zone for all plain specimens with an SLM surface finish (ref. Table 1) are presented in Fig. 10. A residing theme is prevalent among each case; crack initiation is a surface phenomenon. It is inspired by LoF defects that are located within the outer peripheries of a part. This also indicates that internally positioned defects (porosity) in the bulk material play a minimal part in fatigue performance. Indeed, this implies the necessity to obtain a minimum print density of $\sim \mathbf{99.4}$ %, as achieved in this research. Generally, within the field of metal AM, a high density of > 99 % is typically sought after in order to maximise the performance potential of such components.

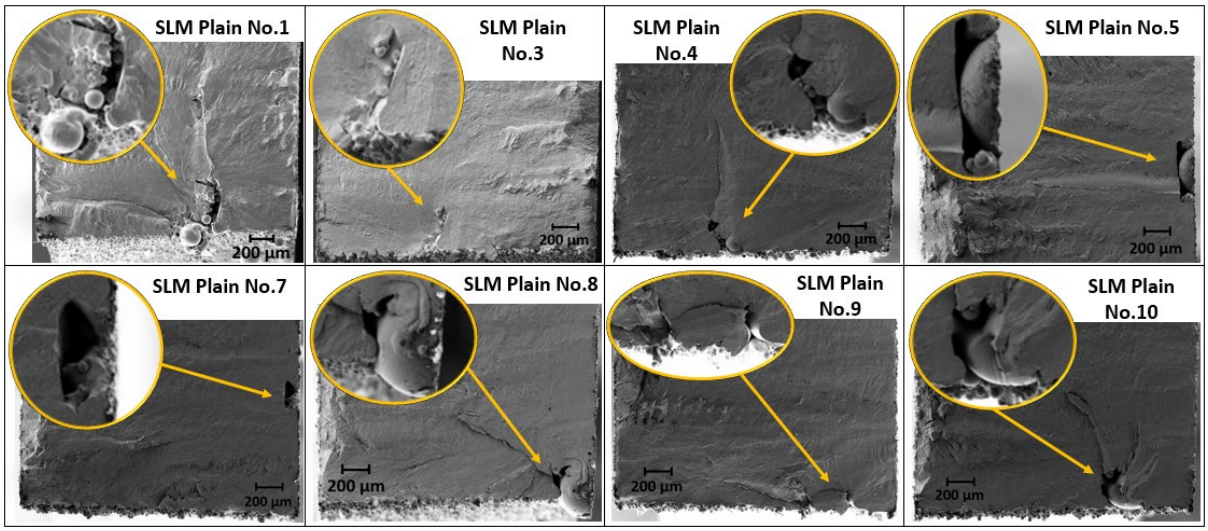

Figure 10 - An overview of fracture surfaces in the slow fracture fatigue zone for all plain specimens with an SLM surface

Upon the observance of plain specimens with a polished surface condition, a similar scenario unveiled itself. Despite the eradication of a rough SLM surface finish, fracture surfaces show the root cause of fatigue onset to be no different. As a case in point, Fig. 11(a) reaffirms this stance. Once again, an LoF defect in touch with the external regions of the specimen is held accountable for the origin of cracking. Hence, regardless of whether a shallow surface polish has been applied or not, crack initiation remains a surface issue. Herein, a magnified stress concentration (Kt) is experienced at a point of weakness (LoF surface defect) within the gauge section of the specimen. This ultimately proves responsible for impending failure. Fig. 4(a) further highlights the innate inability of shallow surface polishing to eliminate process-inherent deficiencies which may be located immediately below the externalities of a part. Therefore, such material inconsistencies remain present and inspire the origin of fatigue. As a remedy to this issue, one possible solution may be to remove a greater volume of material from the externalities of an SLM-manufactured component. In this study, a depth of material with a magnitude that lay within the tens of microns region was eliminated during surface polishing. Further improvements to fatigue resistance may necessitate a larger amount of material to be removed as a way to ensure that no detrimental LoF defects remain connected to the surface periphery. Additionally, it must also be recognised that the material quality of the outer layers can be machine dependant. Consequently, the selection of process parameters in this region must also be carefully considered.

Conversely, notched specimens with a design-induced stress concentration narrate a varied pathway to the inception of failure. The influence of a dominant stress concentration which has been implemented as a consequence of design is clear to see (Fig. 11(b)). This leads to the point of fracture being located along the plane of the notch tip. Therefore, no LoF defect is visible on the fracture surface. It is instead the stress concentration of the geometrically-induced notch that governs fatigue performance.

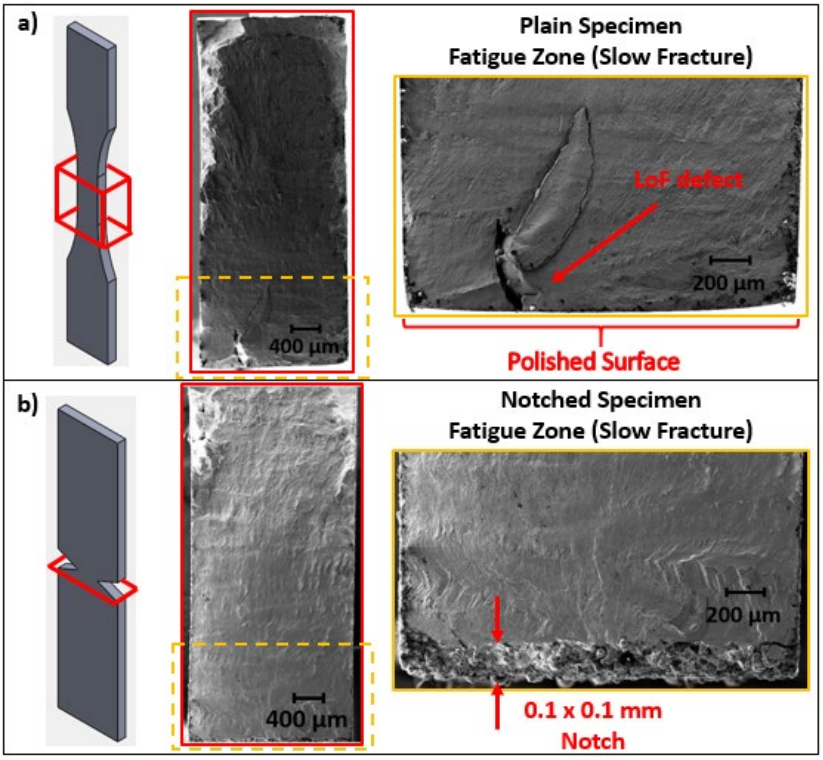

Figure 11 - SEM cross-section of a) polished plain specimen fracture surface situated in the locality of the material's gauge section, initiated by a process-inherent LoF defect and b) notched specimen fracture surface located in the plane of the notch tip, initiated by a design-induced stress concentration

All notched specimens listed in Table 2 failed at the notch location. Citation of the notch-induced stress concentration imparted by such designs was therefore held responsible for crack initiation and subsequent fracture. For specimen designs where $D \leq 0.3$ mm, an increased number of experimental trials (ref. Table 3 – data set size) were conducted for better clarification of results, due to the reduced stress concentration of such components. Nevertheless, upon further reflection, it was recalled that several invalid fatigue tests were made during the use of specimens with the smallest notch size of $D = 0.1$ mm only. Given that all notch sizes of $D \geq 0.3$ mm failed at the notch tip, it serves as a clear signal that incisions equal to or beyond this magnitude in size unquestionably provided the greatest stress concentration within the part. Meanwhile, this cannot be said with reference to those notches where $D = 0.1$ mm. It is hereby suggested that stress-rising hot spots caused by notches of this smaller size scale begin to match those that are produced by process-inherent material defects. Such a hypothesis is further supported by illustrations in Fig. 3. It reiterates the fact that notch sizes of $D = 0.1$ mm begin to possess feature sizes that approach levels of comparable magnitude to those of typical SLM-inherent material characteristics. Such detrimental material anomalies may be present on the immediate surface level in the form of roughness (Fig. 3), or at the sub-surface level in the way of LoF defects (Fig. 4(a)/Fig. 11(a)).

Conclusions

The presence of process inherent defects within SLM Ti-6Al-4V material is well established. However, as previously documented in [38], two differing forms of TCD methods (PM and LM) display sufficient accuracy in predicting the fatigue limit of notched components. This includes modelling an irregular SLM surface as a micro-crack notch for the implementation of TCD methods. The revelation of further investigations in this publication have resulted in additional key findings:

- While both PM and LM techniques of the TCD have acceptable levels of precision, evidence would suggest an enhanced accuracy on behalf of the LM approach.

- SEE analysis confirms that the predictive ability of TCD models primarily fall within experimental error margins. However, this does not hold true for the PM in the case of smaller notched specimens.
- Considering the critical distance parameter, L, regression analysis showed no statistically significant relationship between it and fatigue life.
- With respect to notch geometry, statistical methods showed no influential variation of L with notch radius. Meanwhile, a correlation between notch depth and L was indicated for the case of the PM only, whereby L noticeably increased with notch depth.
- In relation to the onset of fatigue, fracture surfaces signify that even for plain specimens with a polished surface finish (Fig. 10), crack initiation remains a surface related phenomenon in AM material.
- Referring to notched specimens where D=0.1 mm, failure did not consistently arise at the notch location. This indicates that notches of this magnitude begin to align with the severity of those defects that are produced as a result of typical AM material deficiencies.

In summary, results support the adoption of TCD methods as an effective way to quantify the fatigue performance of as-made Ti-6Al-4V, upon which applications of an industrial nature may prosper from. Finally, with respect to improving the overall fatigue resistance of SLM components, it is acknowledged that the composition of material that is situated at the outermost layers of a part requires further attention to detail going forward.

Acknowledgements

This publication was developed with the financial support of Science Foundation Ireland (SFI) under grant number 12/RC/2278 and 17/SP/4721. This research is co-funded by the European Regional Development Fund and SFI under Ireland's European Structural and Investment Fund. This research has been co-funded by Johnson & Johnson 3D Printing Innovation & Customer Solutions, Johnson & Johnson Services Inc. We acknowledge the support of Dr. Mark Culleton in particular.

References

[1] Yap CY, Chua CK, Dong ZL, Liu ZH, Zhang DQ, Loh LE, et al. Review of selective laser melting: Materials and applications. Appl Phys Rev 2015;2. https://doi.org/10.1063/1.4935926.

[2] Shipley H, McDonnell D, Culleton M, Coull R, Lupoi R, O'Donnell G, et al. Optimisation of process parameters to address fundamental challenges during selective laser melting of Ti-6Al-4V: A review. Int J Mach Tools Manuf 2018;128:1–20. https://doi.org/10.1016/j.ijmachtools.2018.01.003.

[3] Rao JH, Stanford N. A survey of fatigue properties from wrought and additively manufactured Ti-6Al-4V. Mater Lett 2021;283:128800. https://doi.org/10.1016/j.matlet.2020.128800.

[4] Wycisk E, Solbach A, Siddique S, Herzog D, Walther F, Emmelmann C. Effects of defects in laser additive manufactured Ti-6Al-4V on fatigue properties. Phys Procedia 2014;56:371–8. https://doi.org/10.1016/j.phpro.2014.08.120.

[5] Beretta S, Romano S. A comparison of fatigue strength sensitivity to defects for materials manufactured by AM or traditional processes. Int J Fatigue 2016;94:178–91. https://doi.org/10.1016/j.ijfatigue.2016.06.020.

[6] Sanaei N, Fatemi A. Analysis of the effect of defects on fatigue performance of additive manufactured metals. Mater Sci Eng A 2020;785:139385. https://doi.org/10.1016/j.msea.2020.139385.

[7] Greitemeier D, Dalle Donne C, Syassen F, Eufinger J, Melz T. Effect of surface roughness on fatigue performance of additive manufactured Ti–6Al–4V. Mater Sci Technol (United Kingdom) 2016;32:629–34. https://doi.org/10.1179/1743284715Y.0000000053.

[8] Pegues J, Roach M, Scott Williamson R, Shamsaei N. Surface roughness effects on the fatigue strength of additively manufactured Ti-6Al-4V. Int J Fatigue 2018;116:543–52. https://doi.org/10.1016/j.ijfatigue.2018.07.013.

[9] Vayssette B, Saintier N, Brugger C, Elmay M, Pessard E. Surface roughness of Ti-6Al-4V parts obtained by SLM and EBM: Effect on the High Cycle Fatigue life. Procedia Eng 2018;213:89–97. https://doi.org/10.1016/j.proeng.2018.02.010.

[10] Leuders S, Lieneke T, Lammers S, Tröster T, Niendorf T. On the fatigue properties of metals manufactured by selective laser melting - The role of ductility. J Mater Res 2014;29:1911–9. https://doi.org/10.1557/jmr.2014.157.

[11] VanSickle R, Foehring D, Chew HB, Lambros J. Microstructure effects on fatigue crack growth in additively manufactured Ti–6Al–4V. Mater Sci Eng A 2020;795:139993. https://doi.org/10.1016/j.msea.2020.139993.

[12] Benedetti M, Fontanari V, Bandini M, Zanini F, Carmignato S. Low- and high-cycle fatigue resistance of Ti-6Al-4V ELI additively manufactured via selective laser melting: Mean stress and defect sensitivity. Int J Fatigue 2018;107:96–109. https://doi.org/10.1016/j.ijfatigue.2017.10.021.

[13] Teixeira Ó, Silva FJG, Ferreira P. Quality and Residual Stresses of the Ti – 6Al – 4V Parts Produced by Additive Manufacturing 2020.

[14] Taylor D. Applications of the theory of critical distances to the prediction of brittle fracture in metals and non-metals. ECF15, 2004.

[15] Neuber H. Theory of notch stresses: principles for exact calculation of strength with reference to structural form and material. 2nd Editio. 1958.

[16] Peterson RE. Notch Sensitivity. Met Fatigue 1959:293–306.

[17] Whitney JM, Nuismer RJ. Stress Fracture Criteria for aminated Composites Containing Stress Concentrations 1974.

[18] Lazzarin P, Tovo R, Meneghetti G, Atzori B. Fatigue crack initiation and propagation phases near notches in metals with low notch sensitivity. Int J Fatigue 1997;19:647–57. https://doi.org/10.1016/S0142-1123(97)00091-1.

[19] Taylor D. Geometrical effects in fatigue: a unifying theoretical model. Int J Fatigue 1999;21:413–20. https://doi.org/10.1016/S0142-1123(99)00007-9.

[20] Tanaka K. Engineering formulae for fatigue strength reduction due to crack-like notches. Int J Fract 1983;22:39–46. https://doi.org/10.1007/BF00942722.

[21] Taylor D. The Theory of Critical Distances: A New Perspective in Fracture Mechanics. 2007.

[22] El Haddad MH, Smith KN, Topper TH. Fatigue crack propagation of short cracks. J Eng Mater Technol Trans ASME 1979;101:42–6. https://doi.org/10.1115/1.3443647.

[23] Murakami Y. Metal fatigue: Effects of Small Defects and Nonmetallic Inclusions. vol. 47. 1991. https://doi.org/10.1115/1.3443343.

[24] Zhang X, Syed AK, Biswal R, Martina F, Ding J, Williams S. High Cycle Fatigue and Fatigue Crack Growth Rate in Additive Manufactured Titanium Alloys. Springer International Publishing; 2020. https://doi.org/10.1007/978-3-030-21503-3.

[25] Hu YN, Wu SC, Wu ZK, Zhong XL, Ahmed S, Karabal S, et al. A new approach to correlate the defect population with the fatigue life of selective laser melted Ti-6Al-4V alloy. Int J Fatigue 2020;136. https://doi.org/10.1016/j.ijfatigue.2020.105584.

[26] Razavi S-M-J, Ferro P, Berto F. Fatigue Assessment of Ti–6Al–4V Circular Notched Specimens Produced by Selective Laser Melting. Metals (Basel) 2017;7:291. https://doi.org/10.3390/met7080291.

[27] Razavi SMJ, Ferro P, Berto F, Torgersen J. Fatigue strength of blunt V-notched specimens produced by selective laser melting of Ti-6Al-4V. Theor Appl Fract Mech 2018;97:376–84. https://doi.org/10.1016/j.tafmec.2017.06.021.

[28] Razavi SMJ, Van Hooreweder B, Berto F. Effect of build thickness and geometry on quasi-static and fatigue behavior of Ti-6Al-4V produced by Electron Beam Melting. Addit Manuf 2020;36:101426. https://doi.org/https://doi.org/10.1016/j.addma.2020.101426.

[29] Nicoletto G, Konečná R, Kunz L, Frkáň M. Influence of as-built surface on fatigue strength and notch sensitivity of Ti6Al4V alloy produced by DMLS. MATEC Web Conf 2018;165:02002. https://doi.org/10.1051/matecconf/201816502002.

[30] Kahlin M, Ansell H, Moverare JJ. Fatigue behaviour of notched additive manufactured Ti6Al4V with as-built surfaces. Int J Fatigue 2017;101:51–60. https://doi.org/10.1016/j.ijfatigue.2017.04.009.

[31] Witkin DB, Albright T V., Patel DN. Empirical Approach to Understanding the Fatigue Behavior of Metals Made Using Additive Manufacturing. Metall Mater Trans A Phys Metall Mater Sci 2016;47:3823–36. https://doi.org/10.1007/s11661-016-3501-z.

[32] Benedetti M, Santus C. Notch fatigue and crack growth resistance of Ti-6Al-4V ELI additively manufactured via selective laser melting: A critical distance approach to defect sensitivity. vol. 121. Elsevier Ltd; 2019. https://doi.org/10.1016/j.ijfatigue.2018.12.020.

[33] Van Hooreweder B, Boonen R, Moens D, Kruth JP, Sas P. On the determination of fatigue properties of Ti6Al4V produced by selective laser melting. Collect Tech Pap - AIAA/ASME/ASCE/AHS/ASC Struct Struct Dyn Mater Conf 2012. https://doi.org/10.2514/6.2012-1733.

[34] Al Zamzami I, Razavi SMJ, Berto F, Susmel L. The critical distance method to estimate the fatigue strength of notched additively manufactured titanium alloys. Procedia Struct Integr 2020;28:994–1001. https://doi.org/10.1016/j.prostr.2020.11.114.

[35] Lanning DB, Nicholas T, Haritos GK. On the use of critical distance theories for the prediction of the high cycle fatigue limit stress in notched Ti-6Al-4V. Int J Fatigue 2005;27:45–57. https://doi.org/10.1016/j.ijfatigue.2004.06.002.

[36] Yamashita Y, Ueda Y, Kuroki H, Shinozaki M. Fatigue life prediction of small notched Ti-6Al-4V specimens using critical distance. Eng Fract Mech 2010;77:1439–53. https://doi.org/10.1016/j.engfracmech.2010.04.001.

[37] Wang J, Yang X. HCF strength estimation of notched Ti-6Al-4V specimens considering the critical distance size effect. Int J Fatigue 2012;40:97–104. https://doi.org/10.1016/j.ijfatigue.2011.12.019.

[38] Gillham B, Yankin A, McNamara F, Tomonto C, Taylor D, Lupoi R. Application of the Theory of Critical Distances to predict the effect of induced and process inherent defects for SLM Ti-6Al-4V in high cycle fatigue. CIRP Ann 2021;00:4–7. https://doi.org/10.1016/j.cirp.2021.03.004.